Geothermics 91 (2021) 102027

Contents lists available at ScienceDirect

Geothermics

journal homepage: www.elsevier.com/locate/geothermics

Numerical investigation of barite scaling kinetics in fractures

Morgan Tranter [a,b,*], Marco De Lucia [a], Michael Kühn [a,b]

[a] GFZ German Research Centre for Geosciences, Fluid Systems Modelling, Telegrafenberg, 14473 Potsdam, Germany
[b] University of Potsdam, Institute of Geosciences, Karl-Liebknecht-Str 24–25, 14476 Potsdam-Golm, Germany

ARTICLE INFO

Keywords:
Geothermal
Fracture sealing
Reactive transport
Geochemical modelling
Crystal nucleation
PHREEQC

ABSTRACT

Barite stands out as one of the most ubiquitous scaling agents in deep geothermal systems, responsible for irreversible efficiency loss. Due to complex parameter interplay, it is imperative to utilise numerical simulations to investigate temporal and spatial precipitation effects. A one-dimensional reactive transport model is set up with heterogeneous nucleation and crystal growth kinetics. In line with geothermal systems in the North German Basin, the following parameters are considered in a sensitivity analysis: temperature (25 to 150 °C), pore pressure (10 to 50 MPa), fracture aperture (10^{-4} to 10^{-2} m), flow velocity (10^{-3} to 10^{0} m s^{-1}), molar volume (50.3 to 55.6 cm^3 mol^{-1}), contact angle for heterogeneous nucleation (0° to 180°), interfacial tension (0.07 to 0.134 J m^{-2}), salinity (0.1 to 1.5 mol kgw^{-1} NaCl), pH (5 to 7), and supersaturation ratio (1 to 30). Nucleation and consequently crystal growth can only begin if the threshold supersaturation is exceeded, therefore contact angle and interfacial tension are the most sensitive in terms of precipitation kinetics. If nucleation has occurred, crystal growth becomes the dominant process, which is mainly controlled by fracture aperture. Results show that fracture sealing takes place within months (median 33 days) and the affected range can be on the order of tens of metres (median 10 m). The presented models suggest that barite scaling must be recognised as a serious threat if the supersaturation threshold is exceeded, in which case, large fracture apertures could help to minimise kinetic rates. The models further are of use for adjusting the fluid injection temperature.

1. Introduction

Deep geothermal systems are a potential source of renewable energy, which is becoming increasingly important in the context of the German energy transition. Numerous pilot projects have shown that significant thermal energy or even electricity is available in a couple of regions in Germany, such as the Molasse Basin, the Upper Rhine Graben (URG), and parts of the North German Basin (NGB, Seibt et al., 2010). In order for them to be used in an efficient operation for energy production, the down-hole temperature should exceed at least 100 °C. In Germany, depending on the local geothermal gradient, these temperatures are expected to be encountered at depths of more than 1800 m (Stober et al., 2013). Sufficient productivity and injectivity are also required for an economical plant. The target reservoir's properties in this regard are porosity and permeability, hence the local geology is decisive in this context. While promising temperatures are met at practicable depths in regions of the NGB (Stober et al., 2013), non-sufficient rock permeabilities in related sedimentary horizons are potentially an issue (Wolfgramm et al., 2008). Previous concepts and applications, for example at the geothermal test-site Groß-Schönebeck located in the NGB (Zimmermann et al., 2010), require enhancing the fracture network by hydraulic stimulation. However, decreasing productivity and injectivity are observed over time. Blöcher et al. (2016) propose that this may be explained by the following processes: accumulation of mineral scaling in the reservoir and the wellbore, thermo-mechanically induced fracture closing, and two-phase flow as a consequence of outgassing. There is evidence that chemical reactions are accountable for reduced injectivity (Scheiber et al., 2013; Stober et al., 2013; Regenspurg et al., 2015; Blöcher et al., 2016; Griffiths et al., 2016).

Precipitation of certain minerals, termed scaling in this context, is a key issue for many geothermal sites in Germany. This is due to the chemical characteristics of the formation waters as well as the perturbation of the system due to changing temperature and pressure during production and re-injection. Total dissolved solids (TDS) of basinal brines in the NGB are correlated with depth, temperature, and corresponding stratigraphical units. The chemistry of these brines are dominated either by Na and Cl or by Na, Ca and Cl, and their TDS range from (100 to 400) g l^{-1}, increasing with depth and temperature (Tesmer et al.,

* Corresponding author at: GFZ German Research Centre for Geosciences, Fluid Systems Modelling, Telegrafenberg, 14473 Potsdam, Germany.
E-mail address: mtranter@gfz-potsdam.de (M. Tranter).

https://doi.org/10.1016/j.geothermics.2020.102027
Received 25 October 2019; Received in revised form 3 December 2020; Accepted 14 December 2020
Available online 23 December 2020

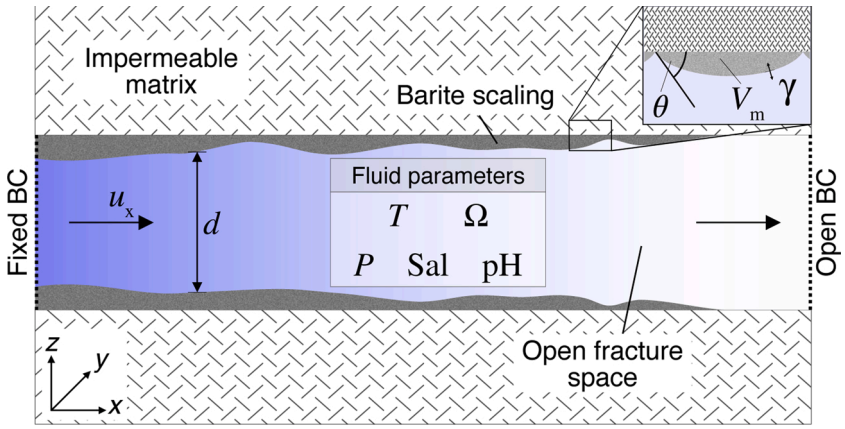

Fig. 1. Conceptual model for the reactive transport setup of the one-dimensional fracture flow between two plates with smooth, impermeable walls. Barite scalings are assumed to accumulate on fracture walls. The following parameters are shown: fracture aperture (d), flow velocity (u_x), temperature (T), pressure (P), pH, saturation state of barite (Ω), fluid background salinity (Sal), molar volume (V_m), contact angle (θ) and interfacial tension (γ).

2007; Wolfgramm et al., 2011b; Stober et al., 2013). Scaling has a damaging and potentially lasting effect by accumulating and hence clogging parts of the system, e.g., the wells, the surface equipment, and notably the reservoir itself.

In regions of the NGB and the URG, brines produced at geothermal sites from depths of 2000 m and more have increased concentrations of Ba (Wolfgramm et al., 2011a), coinciding with observed scalings consisting predominantly of barite (Wolfgramm et al., 2011b,a; Scheiber et al., 2013; Regenspurg et al., 2015). In this regard, barite is the focus of many current investigations (e.g., Scheiber et al., 2013; Bozau et al., 2015; Regenspurg et al., 2015; Griffiths et al., 2016; Heberling et al., 2017). They stand out to be exceptionally hard to remove once accumulated, as no economically viable solvents are available. Although nucleation and crystal growth kinetics of barite have been studied for many years (e.g., Fernandez-Diaz et al., 1990; Christy and Putnis, 1993; He et al., 1995; Dove and Czank, 1995; Kühn et al., 1997; Scheiber et al., 2013; Prieto, 2014; Zhen-Wu et al., 2016), its formation in relation to temperature and pressure change along a geothermal system path still need to be resolved. It is a necessity for plant operation that temporal and spatial precipitation effects of barite can be anticipated so as the right prevention measures can be taken.

The aim of this study is to investigate the role of barite scaling associated to fracture sealing and reduced fracture permeability near the injection well. It further provides the basis for designing complementary fracture permeability investigations on the laboratory scale, similar to Blöcher et al. (2019). The main questions addressed here are its adverse effect on the injectivity of a geothermal system and the sensitivity in terms of the parameters that control precipitation kinetics. For assessing the overall impact on fracture permeability, the critical time t_{crit} for permeability to decrease by one order of magnitude as well as the saturation length scale (SLS) are used as key figures. Numerical, one-dimensional Darcy flow simulations of coupled transport and geochemical processes are carried out on the laboratory scale. Specifically, precipitation is studied by heterogeneous nucleation on the fracture wall and subsequent bulk crystal growth kinetics. The results of a global sensitivity analysis are presented and discussed with regard to their implications for geothermal applications.

2. Methods

2.1. Model setup

A one-dimensional, numerical reactive transport model was set up with a sequential non-iterative approach, consisting of advective solute transport and chemical kinetic reactions.

The conceptual model adopted for the present study is in accordance with experimental core flooding set-ups, where the cores exhibit a single fracture, similar to laboratory and modelling experiments carried out by Blöcher et al. (2019). Laminar, single-phase flow between two plates with smooth, impermeable walls was assumed and hence a single-continuum approach was chosen (Fig. 1). The model domain was discretised in the flow direction ($\Delta x = 3 \times 10^{-2}$ m, six nodes). As only the free fracture space was considered, the geometry of the whole domain is effectively a cuboid of the size ($x \times y \times d$), where the sample length is $x = 0.15$ m, the fracture width is $y = 0.10$ m, and the distance between the plates, i.e. the fracture aperture, is d.

The one-dimensional flow-field was imposed with a homogeneous flow velocity u_x and kept constant throughout the simulation. Advection was assumed to be the dominant solute transport process. Hydro-mechanical diffusion as well as thermal and density driven transport processes were neglected for flow through the fracture. Conservation of mass was numerically solved with an explicit finite differences scheme using first-order upwind. The time step length Δt was chosen so that the Courant-Friedrichs-Lewy condition is always satisfied ($|\frac{u_x \Delta t}{\Delta x}| \leq 1$). Four species were considered in solute transport (see below). The initial and boundary conditions where implemented as follows: solute concentrations and solids in the model domain are initially set to zero. Solute concentrations at the inlet are fixed and the outlet was set to an open flux boundary condition.

2.2. Geochemical modelling

Geochemical batch reaction calculations were carried out using the PHREEQC software package, version 3.5.0 (Parkhurst and Appelo, 2013) and its module IPhreeqc (Charlton and Parkhurst, 2011). During a transport simulation, the chemical state of each node at each time step is passed on to PHREEQC, where a batch kinetic reaction is calculated. The results are then passed back to the transport simulator.

The chemical system implemented was kept to a minimum in order to illustrate the effects of barite precipitation on fracture permeability. Barite precipitation was considered the sole phase transition reaction:

$$SO_4^{2-}(aq) + Ba^{2+}_{(aq)} \rightarrow BaSO_{4\,(solid)} \quad (1)$$

Therefore, the dissolved species Ba^{2+} and SO_4^{2-}, as well as H^+ and e^- were transported. Note that for solute transport, total Ba and S concentrations were treated as though their only species are Ba^{2+} and SO_4^{2-}, respectively, which is valid for the redox and pH state considered. H^+ and e^- virtually stayed constant, but were nevertheless considered as PHREEQC needs them as an input (as pH and pe) and to have a generally valid model. All other dissolved species were kept constant.

The saturation state Ω of barite in a solution is defined as:

$$\Omega_{\text{barite}} = \frac{a_{Ba^{2+}}\, a_{SO_4^{2-}}}{K_{\text{sp,barite}}} \tag{2}$$

where a denotes the activities of the respective species denoted in the subscript and $K_{\text{sp,barite}}$ is the solubility constant of barite. The subscript barite will be omitted hereafter. If $\Omega < 1$, then the fluid is undersaturated, and if $\Omega > 1$, then the fluid is supersaturated with respect to barite and precipitation becomes possible from a thermodynamic point of view. The saturation state was calculated with PHREEQC using the database supplied *pitzer.dat* (Parkhurst and Appelo, 2013; Appelo et al., 2014), where the activities are calculated from concentrations and activity coefficients derived from the Pitzer ion-interaction approach (Pitzer, 1973). The Pitzer approach is known to produce more accurate estimates than the extended Debye-Hückel approach especially at high ionic strengths (Appelo et al., 2014). Indeed, making use of the underlying activity model as well as the temperature and pressure dependent correction of the solubility constant (Parkhurst and Appelo, 2013; Appelo, 2015), Hörbrand et al. (2018) have shown that using *pitzer.dat* yields the best results at conditions relevant to the present case (see below).

2.3. Classical nucleation theory

Based on classical nucleation theory (CNT), the nucleation rate J ($m^{-3}\,s^{-1}$) for homogeneous nucleation (HON) is given by (Nielsen, 1964):

$$J = \Gamma exp\left(-\frac{\Delta G_c}{k_B\, T}\right) \tag{3}$$

where Γ ($m^{-3}\,s^{-1}$) is a pre-exponential factor that quantifies the diffusive flux of molecules to the growing cluster, ΔG_c (J) is the free energy change, k_B ($1.381 \times 10^{-23}\,J\,K^{-1}$) is Boltzmann's constant, and T (K) is the temperature. Changing the supersaturation in a solution potentially has an immense impact on the nucleation rate because it significantly determines ΔG_c as a log function in the denominator (Nielsen, 1964):

$$\Delta G_c = \frac{\beta\, V_m^2\, \gamma^3}{k_B\, T\, ln\Omega} \tag{4}$$

where β is a shape factor depending on the nucleus geometry (here $\frac{16\pi}{3}$, as a sphere was assumed), V_m ($m^3\,mol^{-1}$) is the molar volume, and γ ($J\,m^{-2}$) is the interfacial tension. There are various propositions to approximate Γ (e.g., Nielsen, 1964; Lasaga, 1998; Kashchiev, 2000). Nielsen proposes the following:

$$\Gamma = \frac{2\, D_{\text{mol}}}{d_{\text{ion}}^5} \tag{5}$$

where D_{mol} ($\approx 10^{-9}\,m^2\,s^{-1}$) is the diffusion coefficient, and d_{ion} ($\approx 10^{-9.5}\,m$) is taken as the mean diameter of an ion. Prieto (2014), on the other hand, applied the approach proposed by Kashchiev, which takes additional parameters into account, such as available monomers and sites for nucleation. The Nielsen-approach was adopted for the present study, as fewer uncertain parameters need to be assumed.

If a substrate is in contact with the solution, the formation of a nucleus at the interface is termed heterogeneous nucleation (HEN). In this case, the energy barrier to form a stable nucleus at the phase boundary is lowered as a function of its contact angle θ:

$$\Delta G_{c,\text{HEN}} = \Delta G_c f(\theta). \tag{6}$$

This is due to a higher structural similarity between nucleus and substrate compared to nucleus and solution, and effectively results from tensional forces between each the solid, fluid, and crystal phases. A spherical droplet nucleus was assumed, hence the reduction factor was calculated as (Lasaga, 1998):

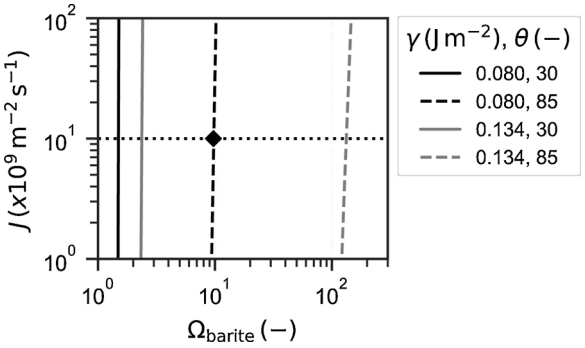

Fig. 2. Schematic illustration of the influence of interfacial energy (γ) and contact angle (θ) on the heterogeneous nucleation rate (J) using Eqs. (3)–(7). Temperature was set to 60 °C. Vertical curves imply that a supersaturation threshold Ω_{thresh} can be assumed. It is often arbitrarily set to the point, where $J = 10^{10}\,m^{-2}\,s^{-1}$ (dotted line). Hence for $\gamma = 0.08\,J\,m^{-2}$ and $\theta = 85°$, Ω_{thresh} is about 10 (diamond marker).

$$f(\theta) = \frac{1}{4}\,(2 - -3\,cos\theta + cos^3\theta) \tag{7}$$

Another overall decisive parameter is the interfacial tension γ, which is demanding to quantify experimentally and is only scarcely available in the literature for barite in respective solutions. Reported values range from 0.08 to $0.134\,J\,m^{-2}$ (Nielsen and Söhnel, 1971; Fernandez-Diaz et al., 1990; He et al., 1995).

In any case, it becomes clear that, compared to HON, a lower supersaturation threshold (Ω_{th}) suffices for HEN to take place. Hence, if a substrate is in contact with the solution, HEN is likely to be the dominant nucleation process. It has been shown experimentally that this is the case for barite at saturation conditions $\log \Omega_{\text{barite}} < 3$ (Poonoosamy et al., 2020a). For the present case this is relevant, as the fracture walls were considered as substrate material. However, the value of the relevant parameter θ is uncertain, as it theoretically depends on the minerals accessible to the solution. Even though He et al. (1995) report a standard value of 0.4 for $f(\theta)$, the whole range from 0 to 1 was considered here, as it describes an uncertain process. Other studies also treat it as a fitting parameter (Liu, 1999; Prieto, 2014; Poonoosamy et al., 2016). Fig. 2 illustrates, how vast the impact of the two parameters γ and θ can be on the heterogeneous nucleation rate. It also becomes clear that, depending on these parameters, there is a supersaturation threshold, from which nucleation becomes relevant. It is often (arbitrarily) related to the point, where the nucleation rate is $10^{10}\,m^{-2}\,s^{-1}$ (Lasaga, 1998; Prieto, 2014).

On the basis of the findings above, the size of a nucleus that is potentially stable in solution is dependent on its supersaturation. Only when this critical nucleus radius r_{crit} is overcome, the nucleus becomes thermodynamically stable. r_{crit} is largely dependent on the ratio of the free energies concerning the nucleus' surface and volume. It can be shown that (Lasaga, 1998):

$$r_{\text{crit}} = \frac{2\,\gamma\, V_m}{R\,T\,ln\Omega} \tag{8}$$

In the case of HEN, a nucleus is in contact with a flat surface, hence the resulting surface area in contact with the solution is (Lasaga, 1998):

$$SA_{\text{nucleus}} = 2\,\pi\, r_{\text{crit}}^2\,(1 - cos\theta) \tag{9}$$

During simulations, the accumulated surface area of all nuclei formed was calculated at every time step and for every cell. Considering $SA = \min(SA_{\text{frac}}, SA_{\text{nuclei}})$, the resulting reactive surface area SA for crystal growth was then passed on to PHREEQC. Note the assumption that the reactive surface area and hence chemical reaction was restricted to the fracture surface area ($SA_{\text{frac}} = 2\,\Delta\, x\, y$).

Table 1
Ranges of model parameters chosen for the sensitivity analysis selected to capture expected conditions in a fracture network near an injection well in a geothermal system.

Input parameter	Abbreviation	Unit	Varied ranges	Source
Fracture aperture	d	m	$\log(-3 \pm 1)$	Zimmermann et al. (2010)
Flow velocity	u_x	m s^{-1}	$\log(-1.5 \pm 1.5)$	Zimmermann et al. (2010)
Temperature	T	°C	60 ± 10	Blöcher et al. (2016)
Pressure	P	Pa	$\log(7.35 \pm 0.35)$	Blöcher et al. (2016)
pH	pH	–	6 ± 1	Regenspurg et al. (2015)
Saturation state	Ω	–	16 ± 15	Regenspurg et al. (2015)
Fluid salinity	Sal	mol kgw^{-1} NaCl	0.8 ± 0.7	Zhen-Wu et al. (2016)
Molar volume	V_m	cm^3 mol^{-1}	52.9 ± 2.7	Appelo (2015)
Contact angle	θ	–	90°±90°	Lasaga (1998)
Interfacial tension	γ	J m^{-2}	0.102 ± 0.032	see Section 2.3

2.4. Crystal growth

Precipitation and dissolution reaction kinetics of minerals can be modelled on a macroscopic scale using rate constants derived from bulk reaction experiments. A general form for calculating the precipitation rate was used (Lasaga, 1998):

$$r = -\frac{\mathrm{SA}}{m_{\mathrm{water}}} k\,(1 - \Omega^p)^q \tag{10}$$

where m_{water} (kg) is the mass of water in solution, k (mol m^{-2} s^{-1}) is the rate constant, and the dimensionless exponents p and q are empirical parameters describing reaction order and deviation from equilibrium according to the transition state theory (Lasaga, 1998). Zhen-Wu et al. (2016) currently provide the only source for bulk precipitation rates in NaCl-solutions. They conducted experiments on dissolution and precipitation kinetics of barite in solutions with salinities up to 1.5 mol kgw^{-1} NaCl (kgw = kg water), temperatures from (25 to 90) °C, and pH from 2 to 9. Further, they derived lumped rate constants from this that incorporate temperature, ionic strength, and pH dependent mechanisms, by fitting the experimentally measured time series to Eq. (10), and setting q and p each to unity. More commonly, the reaction rate equation (Eq. (10)) is further decomposed into separate terms, each representing a factor-dependent reaction mechanism. For example, influencing effects at varying pH can be described by using an acid, a neutral, and a base term, or temperature can be represented by using an Arrhenius term (Lasaga, 1998). Based on transition state theory, Palandri and Kharaka (2004) provide a set of rate parameters for calculating kinetic reactions in this fashion for a range of minerals, among them barite. However, since there is only limited data available on precipitation rates at saline conditions (Christy and Putnis, 1993; Dove and Czank, 1995; Zhen-Wu et al., 2016), it was decided to use a more general rate equation. In the present study, rate constants were derived by using data from Zhen-Wu et al. (2016) in order to process calculations on precipitation rates, which was implemented using Eq. (10). An example PHREEQC input file can be found in Appendix (A). For predicting rate constants at varying conditions for the reactive transport models, a linear regression was carried out.

The dimensionless Damköhler number for advective transport quantifies the ratio of a characteristic time for advective transport to a characteristic time for reaction. It therefore gives an indication on the nature of the reaction front with regards to the spatial discretisation. It was calculated with (Steefel, 2008):

$$t_{\mathrm{adv}} = \frac{\Delta x}{u_x} \tag{11}$$

$$t_{\mathrm{react}} = \frac{C_{\mathrm{eq}}}{\mathrm{SA}\,k} \tag{12}$$

$$\mathrm{Da}_{\mathrm{adv}} = \frac{t_{\mathrm{adv}}}{t_{\mathrm{react}}} \tag{13}$$

where C_{eq} is the solubility of barite in equilibrium.

In a homogeneous case, equilibrium is reached within a grid cell if $Da_{\mathrm{adv}} > 1$. From this, the saturation length scale SLS was derived, which describes the flow length, beyond which equilibrium is reached (Steefel, 2008):

$$\mathrm{SLS} = \frac{\Delta x}{\mathrm{Da}_{\mathrm{adv}}} \tag{14}$$

The mean SLS of all nodes was taken as one key figure for the sensitivity analysis (see below) and is an indication for the influencing range of barite scaling around an injection well.

2.5. Permeability evolution

Fracture transmissivity is an important parameter when evaluating the suitability of a target reservoir. To derive a quantifiable value for this, the change of fracture aperture as a consequence of barite precipitation needs to be related to change in fracture permeability K (m^2). Assuming laminar flow and parallel fracture walls, exhibiting smooth surfaces and 'no-slip' boundary conditions, the permeability of a fracture can be approximated with the 'cubic law' (e.g., Neuzil and Tracy, 1981). If a single fracture is considered, it is given as:

$$K_i = \frac{d_i^2}{12} \tag{15}$$

where the subscript i signifies a respective cell in flow direction at a given time. Change in fracture aperture due to barite precipitation was derived by calculating the volume fraction in each cell at each time step and relating it to the initial aperture:

$$d_i = d_0 \left(1 - \frac{n_{\mathrm{i,barite}}\, V_m}{\Delta x\, y\, d_0}\right) \tag{16}$$

where n_{barite} (mol) is the amount of barite, Δx (1×10^{-3} m) is the cell spacing in flow direction, y (0.1 m) is the fracture length (diameter of core), and the subscript 0 signifies the initial state. It follows that the permeability K_i in each cell can then be calculated from the initial permeability K_0:

$$K_i = K_0 \left(\frac{d_i}{d_0}\right)^2 \tag{17}$$

The effective permeability of the whole fracture was then taken as the harmonic mean of the respective permeability in each cell.

For assessing a decisive indicator of the coupled simulations with regards to permeability change, the time for the permeability to change by one order of magnitude was taken as another key figure for the sensitivity analysis (see below). This value was presumed to be the critical time t_{crit} for the fracture to be virtually sealed in the present application, as it would render the geothermal system as uneconomic. It was taken advantage of the fact that the closing rate of the fracture $r_d = \frac{dd}{dt}$ approaches a constant value, since the reactive surface area is limited

Table 2
Geochemistry and state of the formation water in the geothermal reservoir Groß-Schönebeck. The equilibrated column is calculated with PHREEQC (pitzer.dat), where the measured column is the input data, barite was equilibrated ($\Omega = 1$), and charge balance was done with Cl^-. Unit (M) is treated equally as (mol kgw^{-1}). For abbreviations, see Tab 1 .

Parameter	Measured (Regenspurg et al., 2010)	Equilibrated
T	150 °C	150 °C
P	500 bar	500 bar
pH	5.7	5.7
Na^+	1.67 M	1.67 M
K^+	7.40×10^{-2} M	7.40×10^{-2} M
Ca^{2+}	1.35 M	1.35 M
Mg^{2+}	1.80×10^{-2} M	1.80×10^{-2} M
Ba^{2+}	2.50×10^{-4} M	2.88×10^{-3} M
Sr^{2+}	2.20×10^{-2} M	2.20×10^{-2} M
Cl^-	4.71 M	4.52 M
SO_4^{2-}	1.50×10^{-3} M	4.13×10^{-3} M
HCO_3^-	3.10×10^{-4} M	3.10×10^{-4} M

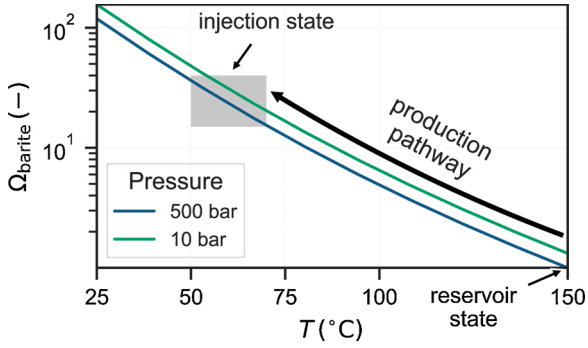

Fig. 3. Expected supersaturation of barite, if temperature and pressure are reduced along the production pathway of a geothermal power plant. It is assumed that the fluid is in equilibrium at the reservoir state ($\Omega = 1$). The grey box highlights the presumed temperature and pressure injection state, which corresponds to a supersaturation in the range of 15–30. (For interpretation of the references to color in this figure legend, the reader is referred to the web version of this article.)

by fracture surface area. If the closing rate is assumed to be constant, it can be shown from Eq. (15) that:

$$t_{crit} = \frac{d_{initial}\left(1 - \frac{1}{\sqrt{10}}\right)}{r_d} \tag{18}$$

A simulation was terminated if either r_d approached a constant value, i.e. the change compared to the previous advection step is smaller 1%:

Table 3
Rate constants for bulk precipitation of barite at varying conditions used for the linear regression. The parameters T and Sal are the input features, which were transformed and scaled for the regression. Comparing experimental and model rates yields $R^2_{adj} = 0.88$.

T	Sal	$log k^a_{exp}$	$\log k_{model}$
°C	mol kgw^{-1} NaCl	mol m^{-2} s^{-1}	mol m^{-2} s^{-1}
25	0.0	−8.46	−8.21
25	0.1	−7.62	−7.99
25	1.0	−7.60	−7.51
25	1.5	−7.55	−7.36
60	0.1	−7.22	−7.09
60	0.7	−6.60	−6.73
60	1.0	−6.54	−6.62
60	1.5	−6.52	−6.46
25	1.0	−7.40	−7.51

(a) Experimental data on bulk precipitation (Zhen-Wu et al., 2016).

$$|1 - \frac{r_{d,t}}{r_{d,t+1}}| < 0.01 \tag{19}$$

Or if no nucleation has taken place at all after at least 18 advection steps (3 × nodes). In the latter case, this would result in $t_{crit} = \infty$, but $t_{crit} = 10^{99}$ s was adopted here in order to have comparable numerical values.

2.6. Sensitivity analysis

A sensitivity analysis was carried out with respect to the model outputs t_{crit} and SLS for assessing the temporal and spatial effects of barite scaling, respectively. The parameters covered and their respective ranges for the present study are summarised in Table 1. All parameters were treated independently from another. For a more complete list, see Table B.5.

The parameters fracture aperture (d), Darcy velocity (u_x), temperature (T), pore pressure (P), pH, and saturation state (Ω) were chosen so as to capture typical values that can be expected in the fracture network near an injection well. For this, the geothermal reservoir Groß-Schönebeck (Zimmermann et al., 2010; Blöcher et al., 2016; Regenspurg et al., 2015) was taken as a reference. The geochemistry of the respective formation water can be seen in Table 2(Regenspurg et al., 2010).

It is assumed that the formation water is in equilibrium with barite in the reservoir. Therefore, the formation water was equilibrated with barite using PHREEQC and the database pitzer.dat. If temperature and pressure is then reduced, as it were produced, the fluid will become supersaturated with respect to barite (Fig. 3). As can be seen, due to a temperature decrease from 150 °C (reservoir state) to 70 °C (injection state), SR is expected to be on the order of 30. The influence of decreasing pressure is noticeably lower. It is furthermore expected that some barite will readily precipitate before the fluids reach the reservoir surrounding the injection well. Hence, scenarios at lower supersaturation were also investigated. Salinity is an important factor for the rate constants introduced and is bound to the respective experimental data. The molar volume (V_m) is given in the Pitzer database (Parkhurst and Appelo, 2013), but it was varied arbitrarily to ±5% in order to account for inhomogeneous scaling morphology along the fracture. The contact angle (θ) was varied within the two limiting cases for heterogeneous nucleation, and the range of the interfacial tension (γ) was obtained from literature data (Nielsen and Söhnel, 1971; Fernandez-Diaz et al., 1990; He et al., 1994; Prieto, 2014).

The relative importance of each parameter was firstly ascertained by a screening method, which illustrates varying effects and processes on a general level. The one-at-a-time (OAT) method of Morris (1991) was utilised for this so as to yield the mean elementary effects and their standard deviation of each parameter in the model output. The sampling is carried out on a regularly spaced grid, varying each parameter at a time. This is done for a limited amount of model runs and is utilised to retain non-influential parameters. The number of model runs results from $t(p + 1)$, where p is the number of parameters and t is the number of trajectories (Morris, 1991). $p = 10$ and t was set to 1000, resulting in 11 000 model runs for the OAT screening.

In a next step, the global, variance based sensitivity analysis of Sobol (2001) was applied, which implements a more elaborate parameter sampling procedure than the OAT method (Saltelli, 2002). From this, the interaction effects and total sensitivity indices for each parameter were derived and they quantify a parameter's total influence on the system. Due to the model termination criteria ($t_{crit} = 10^{99}$ s), the mechanism of HEN potentially conceals parameter dependencies important for governing crystal growth. So as to highlight the effect of crystal growth, noteworthy scenarios at supersaturation 15, 20 and 30 were considered. Further, parameters controlling HEN were fixed at this stage to $\gamma = 0.08$ J m^{-2} and $\theta = 85°$. These standard values proposed by He et al. (1994) result in a threshold supersaturation of $\Omega_{th} \approx 10$ (Fig. 2). This leaves seven factors ($p = 7$) for the global sensitivity analysis. The

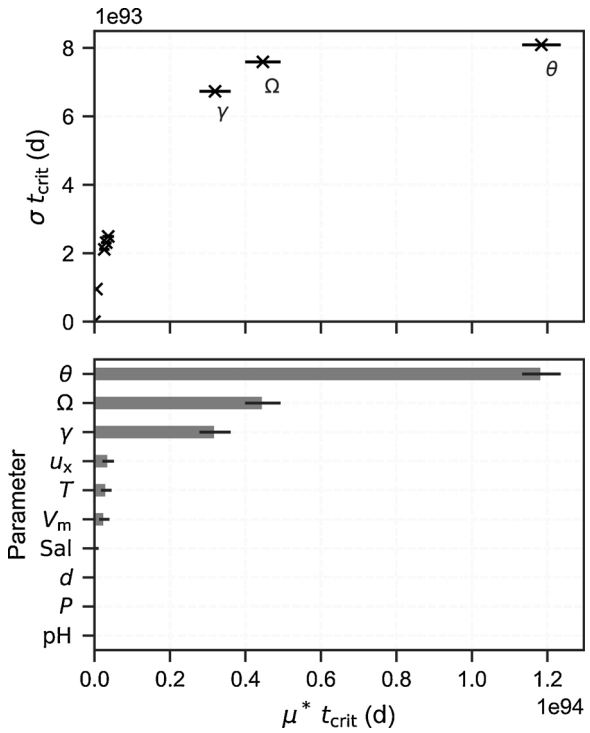

Fig. 4. Absolute mean of the elementary effects (μ^*) and the respective standard deviations (σ) of the model parameters on t_{crit} derived from the one-at-a-time (OAT) method of Morris (1991). The solid, horizontal lines represent bootstrapped confidence intervals of μ^*. The ranges of the model input parameters are shown in Table 1.

number of model runs needed for this follows from $n(2p+2)$, where p is the number of parameters and n is the number of samples (Saltelli, 2002). n was set to 1000, resulting in 16 000 model runs.

3. Results

3.1. Rate constants

The lumped rate constant (k) for evaluating crystal growth rates from Eq. (10) was calculated with a linear regression at respective temperature (T) and salinity (Sal) conditions, as shown in Table 3.

Comparing various first-order linear regression models with interaction terms, to prevent over-fitting given only nine data points are available, the following model yielded the lowest averaged residuals:

$$log k_{model} = k_1\, T^{-1} + k_2\, \mathrm{Sal}^{\frac{1}{2}} + k_3 \tag{20}$$

The regressed coefficients are $k_1 = -0.453$, $k_2 = 0.291$, and $k_3 = -7.279$, with an adjusted $R^2_{adj} = 0.88$. The resulting rate constants using this model at respective experimental conditions are shown in Table 3.

A detailed description of the experimental data is given in Zhen-Wu et al. (2016). In general, k is positively correlated with temperature and ionic strength. The temperature dependency can be described by an Arrhenius term (Lasaga, 1998). Hence, the reciprocal of the temperature was chosen to predict $\log k$. The influence of the ionic strength is much higher at lower salinities. This dependency levels off at higher salinities, therefore the root of salinity for the linear model was used.

The linear model obtained for determining the rate constant was introduced into the reactive transport model. Together with the reactive surface area and the supersaturation, it is the basis for the kinetic crystal growth calculations using Eq. (10) as implemented in PHREEQC.

3.2. Parameter screening

In the parameter screening, the bandwidths of all parameters shown in Table 1 were evaluated. The results of the OAT sensitivity analysis with regard to the temporal model output t_{crit} (Eq. (18)) are shown in Fig. 4. The absolute mean elementary effects ($\mu*_{t_{crit}}$) and respective standard deviations ($\sigma_{t_{crit}}$) of most parameters are high ($>10^{94}$ d), which is due to the model termination criteria. The value 10^{99} s was used as a numerical placeholder, which signifies that t_{crit} is infinite due to negligible crystal growth. Indeed, 9080 of the total 11 000 model runs terminated because no HEN happened at all. Thus, notably the parameters, defining whether the threshold supersaturation (Ω_{th}) is exceeded or not, i.e. supersaturation, contact angle, and interfacial tension, have the strongest impact on the total model outcome. This can be derived from Fig. 4, in which the parameters furthest away from the point of origin are more influential in the parameter space investigated. The elementary effects of the parameters darcy velocity, molar volume and temperature, and salinity are similarly high, but one or two orders lower. In contrast, it becomes apparent that the parameters fracture aperture, pH, and pore pressure only have a comparably small sensitivity. Customarily, the uncertainties of parameters, which have small elementary effects, are neglected in further analyses. But in fact, they are on the order of $\gg$50 years, even though they have near to no impact on the nucleation mechanism. Hence, the model exhibits two distinguishable mechanisms, each depending on different parameters. Both mechanisms have a decisive impact on the model output as the influences are by far higher than the life expectancy of an utilised geothermal system.

3.3. Global sensitivity analysis

The role of the nucleation mechanism is shown to be important in the previous section. For evaluating the sensitivity of crystal growth with respect to the input parameters in more detail, time spans for fracture sealing were examined at a fixed supersaturation threshold ($\Omega_{th} \approx 10$) and three selected supersaturation states (A: $\Omega = 15$, B: $\Omega = 20$, C: $\Omega = 30$.). The distributions of t_{crit} with regard to the input parameters for all scenarios are shown in Fig. 5.

Comparing all three scenarios, it can be seen that the larger the supersaturation is, the smaller t_{crit} is. It should be noted that the time ranges are many orders of magnitude higher for C than for A and B. This becomes apparent through stronger scattering in the lower and especially the upper ranges, i.e. a higher variance. In all scenarios, a negative trend can be seen for the parameters T and Sal, whereas a pronounced, positive trend can be seen for d. For example, in B, the median of t_{crit} at a low fracture aperture of about 10^{-1} mm is approximately only 5 days, whereas for a fracture aperture of 10 mm the median is almost 200 days, about 40 times higher. For A, the respective t_{crit} values are only slightly lower (3 and 140 days), however they are significantly higher ($>$2000 days) for C and virtually independent of the fracture aperture. A slight positive trend can also be ascertained for V_m, though only for C; in A and B no correlation becomes apparent in this sense. Furthermore, pH and P exhibit no indication of correlation in all scenarios.

The distribution of the model results are described with summary statistics, as can be seen in Table 4.

The median values of t_{crit} for scenarios B and C are on the order of tens of days. For scenario A on the other hand it is on the order of years. The negative trend of t_{crit} with respect to supersaturation becomes apparent again, as does the broader range of the outcome with a smaller supersaturation. Therefore, the uncertainty becomes increasingly larger, the closer the supersaturation is to the threshold supersaturation. While the maximum fracture sealing time in C is about 500 days, it is $\gg$50 years in A, suggesting that the variance increases as supersaturation decreases.

The results of the spatial impact, i.e. the distribution of SLS with respect to varying input parameters, are shown in Fig. 6.

For scenarios B and C it becomes clear that the parameters flow

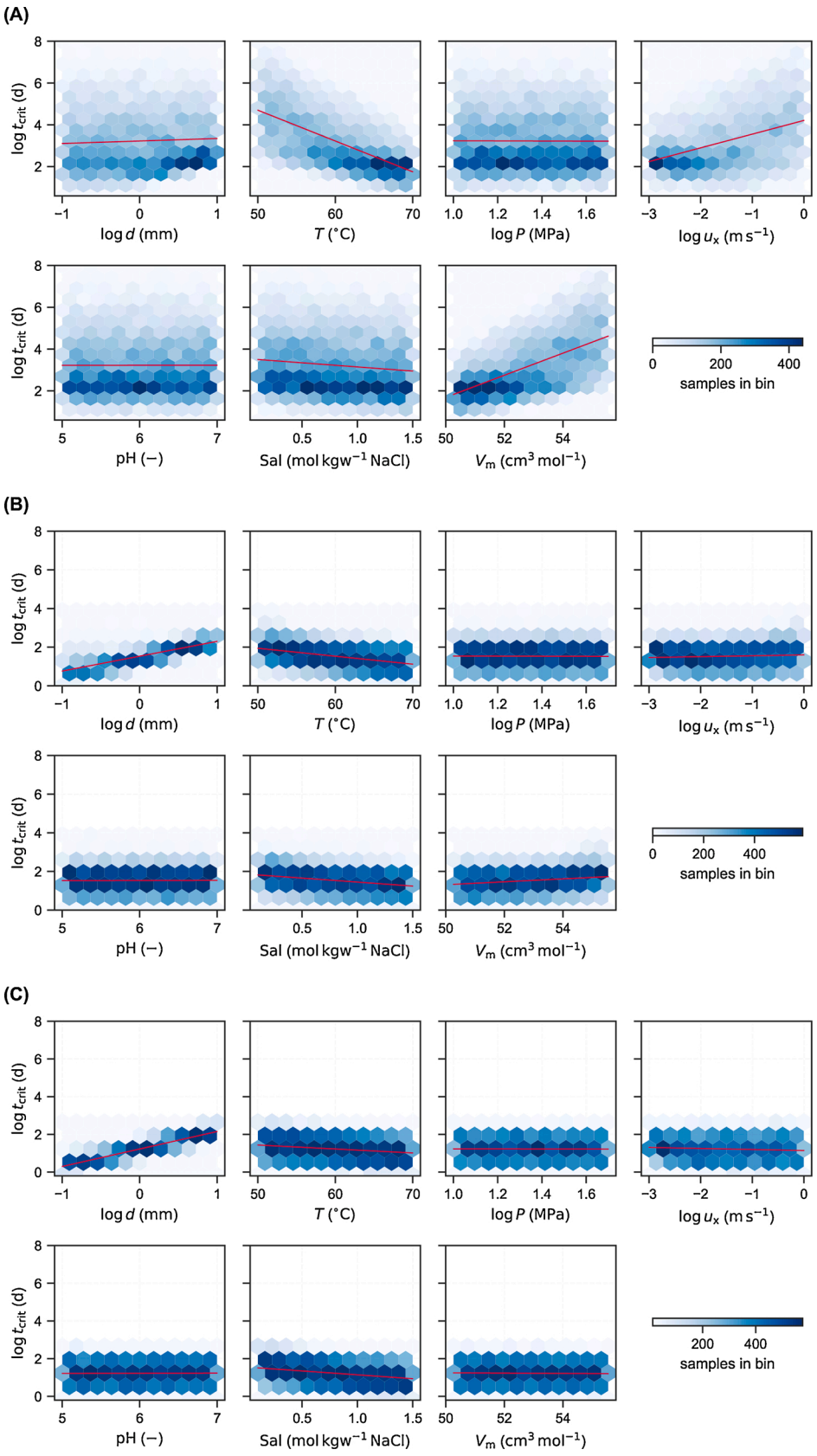

Fig. 5. Distribution of t_{crit} with regard to varying model parameters for 16 000 model runs obtained from the global sensitivity analysis (Sobol, 2001). The sampling implemented is based on Saltelli (2002). The solid lines represent the mean trend obtained from linear regression. The lightness of each hexagon represents the number of results of the model run plotted within the respective area. (A) $\Omega = 15$, (B) $\Omega = 20$, (C) $\Omega = 30$.

Table 4
Quantiles (Q) of the temporal and spatial model output obtained from the global sensitivity analysis (Sobol, 2001) at various fixed supersaturations Ω. They give an indication for when the permeability has decreased by one order of magnitude (t_{crit}) and how far along a fracture is sealed, i.e. the saturation length scale (SLS), due to barite scaling.

Scenario	Ω	Output	25th Q	50th Q	75th Q
A	15		148	804	12,853
B	20	$t_{crit\ (days)}$	12	33	94
C	30		6	16	49
A	15		16	205	7521
B	20	SLS (m)	3	14	92
C	30		2	12	70

velocity u_x and fracture aperture d have by far the largest influence on SLS and that both exhibit a positive correlation. All other parameters appear negligible in these cases. For scenario A, on the other hand, the range of the results is much larger and a strong dependency on T, V_m, and u_x can be seen. While the mean SLS at low velocities ($u_x = 10^{-3}\,m\,s^{-1}$) is about 1 m, it is about 1 km at high velocities ($u_x = 1\,m\,s^{-1}$). The describing statistics referring to this are also provided in Table 4. SLS is in the range of tens of metres for scenarios B and C. For scenario A, it is in the range of hundreds of metres or even kilometres and the uncertainty is also much larger.

As a primary result of the global sensitivity analysis, the first-order S_i and total interaction indices S_{Ti} of the model input parameters were derived (the subscript i signifies the respective parameters in this case). In Fig. 7, they are shown with respect to the model output t_{crit} for all three scenarios. As S_i signifies the contribution of a parameter i on the output variance by itself, it can be used to prioritise the input parameters. To evaluate, which parameters are rather non-influential and to also capture possible non-linear effects on the model output variance, S_{Ti} is used, which includes further interaction between the parameters. If S_{Ti} is negligibly small, the respective parameter can be assumed to be non-influential in this context. Generally, scenario C exhibits very different parameter dependencies than A, while B can be described as a transition scenario. In C, the model parameters temperature, flow velocity, molar volume and salinity have the highest impact on S_i. Combined, they only add up to 3% of the total variance of the model output, therefore significant variance is due to non-linear and interaction effects among the parameters, which is quantified by the respective S_{Ti} values. In all scenarios, pH and pore pressure have sensitivity indices of 0, hence they have no impact on the model output. In scenario C, the most sensitive parameter is the fracture aperture, which makes up for over 65% of the variance of the output by itself. To a slight extent, salinity and temperature also have an impact, although $S_{T,sal}$ and $S_{T,T}$ are both below 0.1, indicating at least some interaction. In total, S_i accumulates to approximately 0.8, hence the variance of the model output can mostly be explained by varying the parameters on their own and interaction effects are rather small. Scenario B appears to be somewhere between scenario A and C with regard to the parameter dependencies.

The sensitivity indices for the saturation length scale SLS are slightly differently distributed (Fig. 8). Here, scenario A and B reveal quite similar dependencies on T, u_x and V_m, with near to no primary interaction, but complex parameter interplay. For scenario C, on the other hand, apart from temperature, which has a minimal influence ($S_{T,T} = 0.01$), only flow velocity and fracture aperture determine the model output. All other parameters have a negligible influence. The first-order indices of flow velocity and fracture aperture combined make up for 40% of the variance of the model output. The rest of the variance is primarily determined by interaction effects between these two parameters. Flow velocity and fracture aperture therefore are the most influential parameters for the influencing range along a fracture at higher supersaturation. At lower supersaturation, the parameter dependencies are not as clear.

3.4. Scenario Groß-Schönebeck

In the sensitivity analyses, all parameters were treated independently from one another. Some parameters that were fixed this way, however, may be dependent on others in a true case scenario. To illustrate the effect of coupled nucleation and crystal growth in a case where supersaturation is dependent on lowering temperature, we applied this model to the Groß-Schönebeck site. Here, the equilibrated fluid chemistry was taken as the input condition (Table 2). The temperature was varied from 25 to 150 °C, and the fracture aperture was varied from 0.1 to 10 mm. All other parameters were kept constant (B.5). The resulting times for permeability of a fracture to decrease by one order of magnitude (t_{crit}) are shown in Fig. 9. Similarly to the previous results, it becomes clear that larger apertures exhibit larger t_{crit}. For small apertures (<1 mm), this is in the range of days, but for larger apertures, this is in the range of months. Three distinct domains on the temperature scale can be seen here. Decreasing the temperature from 150 °C to approximately 90 °C, nucleation begins, as the supersaturation threshold is exceeded. This coincides with a supersaturation of about 10 (Fig. 3). Cooling further down, nucleation rate continues to become stronger up to a point, where nucleations will quickly cover the whole fracture surface (from about 70 °C downwards). From then on, supersaturation will further increase, but the kinetic rate constant, on the other hand, decreases. It can be seen that t_{crit} becomes larger again, which can be attributed to the fact that the kinetic rate constant decreases more strongly than supersaturation increases with regards to Eq. (10).

4. Discussion

Scaling is a common issue in geothermal systems, as scales may form in the wells and the surface system, but also in the reservoir. Barite is assumed to be originally in equilibrium with the reservoir fluids, since reservoir rock samples contain barite (Regenspurg et al., 2015). As temperature and pressure decrease during production, the solubility of barite also decreases (Fig. 3), triggering the emergence of barite precipitates along the system pathway. In a continuous production-injection cycle, fluids cool down, while passing through the surface system, after which they are re-injected back into the reservoir through the injection well at about (50 to 70) °C (Zimmermann et al., 2010; Griffiths et al., 2016). The hypothesis is that scales may accumulate in the reservoir behind the injection well over time, if supersaturated fluids are constantly re-injected. This would eventually result in decreased permeabilities and likewise reduced injectivities over time; a highly unwanted effect as there is no solvent applicable for barite available. It is expected that mineral scales will also form before the fluids reach the reservoir, where supersaturation is the highest. Fluids will most likely have their steepest supersaturation gradient somewhere in the surface system near the production well or the heat exchanger. However, due to the low specific surface area compared to the fracture space, the formation of nuclei and subsequently crystal growth kinetics is assumed to be attenuated. Even if nuclei form in the surface system, they may be “washed” into the reservoir. Therefore, longer shut-in periods potentially pose a problem in this context because in this case there is more time for nuclei to form larger clusters, settle on surfaces, and become immobile. Barite scales have been observed to form in the injection well of the geothermal site Soultz-sous-Forêts (Scheiber et al., 2013), but also to completely seal fractures in this context (Griffiths et al., 2016), supporting the hypothesis.

Numerical experiments were conducted for evaluating under which circumstances barite scales can form and if they potentially have an impact on fracture permeability on a time-scale of a geothermal power plant’s life time. This was carried out for fractures on the laboratory scale as a precursor to laboratory experiments, but it can be transferred to reservoir scales. In order to capture the high dynamics of a geothermal system and to make estimations on spatial and temporal impacts, a coupled kinetics model was employed. The novel approach is that

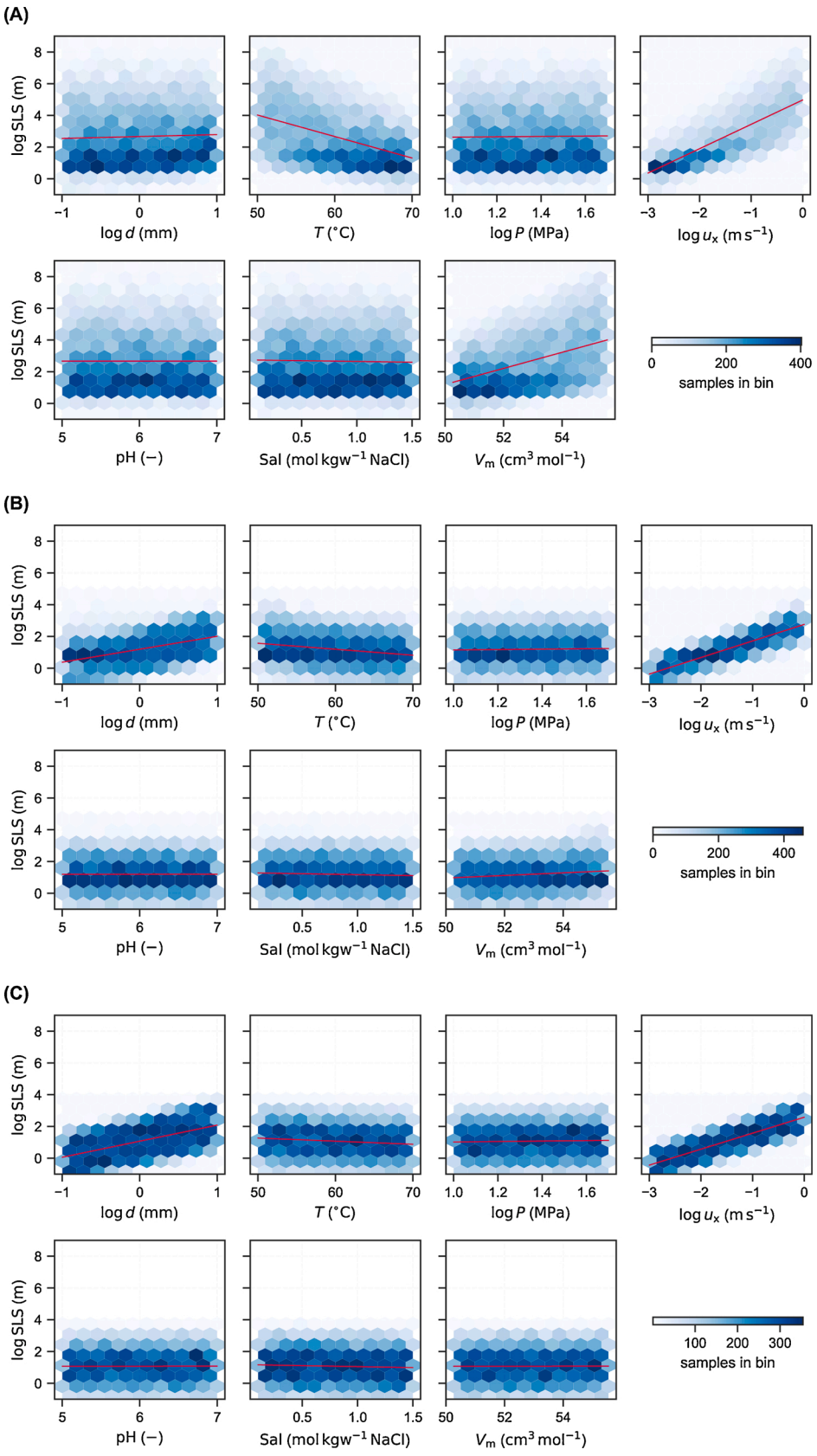

Fig. 6. Distribution of SLS with regard to varying model parameters for 16 000 model runs obtained from the global sensitivity analysis (Sobol, 2001). The sampling implemented is based on Saltelli (2002). The solid lines represent the mean trend obtained from linear regression. The lightness of each hexagon represents the number of results of the model run plotted within the respective area. (A) $\Omega = 15$, (B) $\Omega = 20$, (C) $\Omega = 30$.

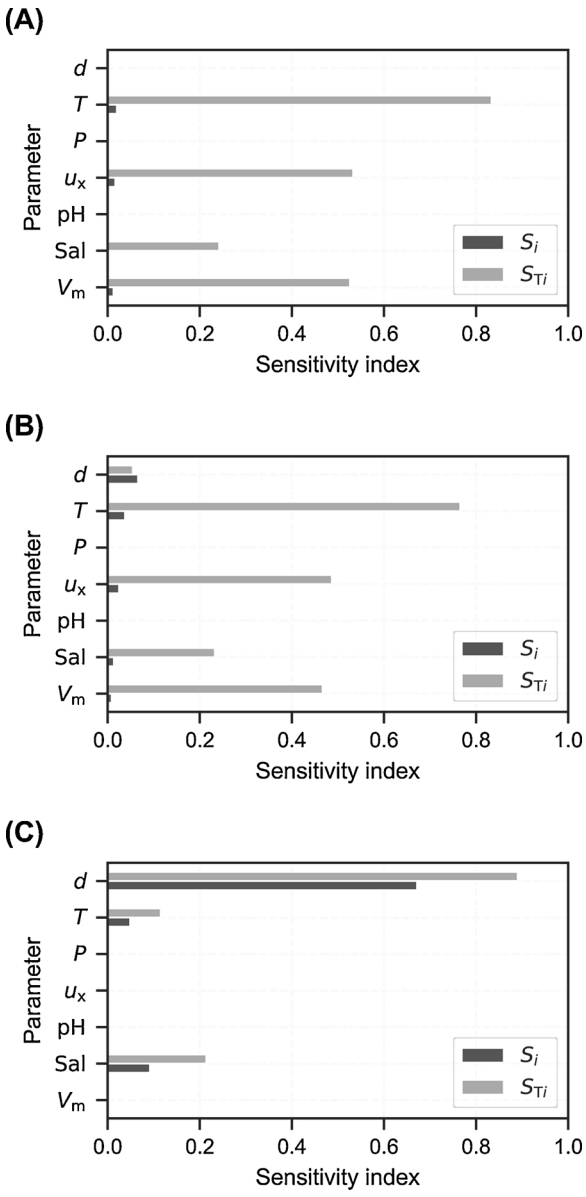

Fig. 7. First-order S_i and total interaction indices S_{Ti} of the model input parameters with respect to the model output t_{crit}. All values are derived using the variance-based sensitivity analysis based on Sobol (2001). (A) $\Omega = 15$, (B) $\Omega = 20$, (C) $\Omega = 30$.

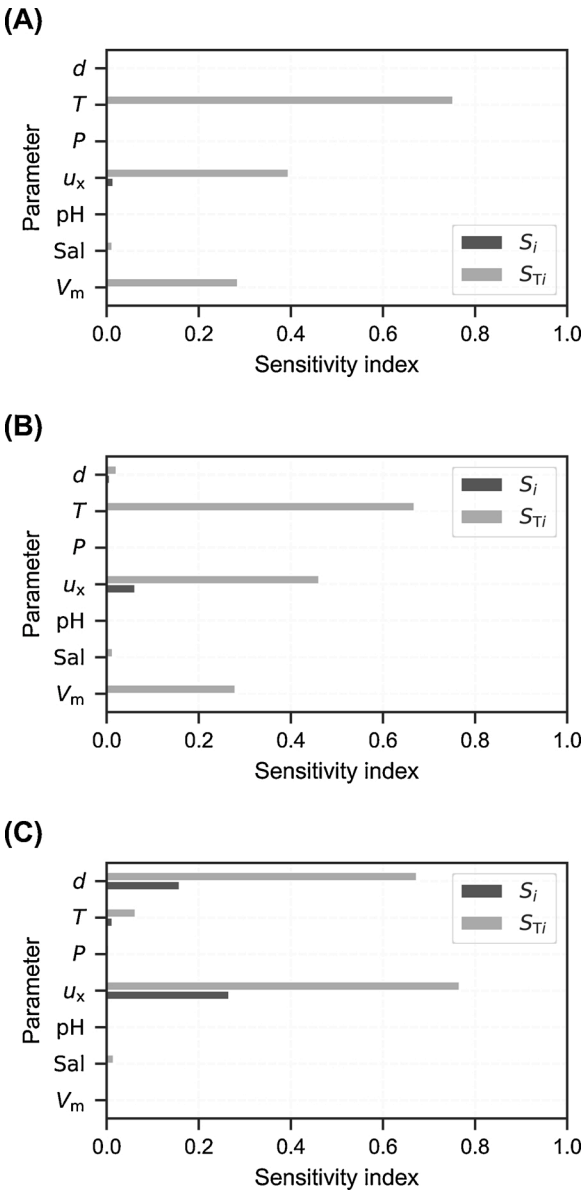

Fig. 8. First-order S_i and total interaction indices S_{Ti} of the model input parameters with respect to the model output SLS. All values are derived using the variance-based sensitivity analysis based on Sobol (2001). (A) $\Omega = 15$, (B) $\Omega = 20$, (C) $\Omega = 30$.

nucleation on fracture walls as well as crystal growth is taken into account. Other related studies either use an ad hoc precursor crystal surface, thereby circumventing the nucleation mechanism, or simply just use thermodynamics (e.g., Bozau et al., 2015; Griffiths et al., 2016).

The quantities and parameters required for making reliable predictions are to some extent uncertain or variable. A global sensitivity was carried out, using the key figures t_{crit} (Eq. (18)) for the time scale and SLS (Eq. (14)) for the range of influence of fracture sealing. System parameters are hereby highlighted that are either under-determined or that are most sensitive for the processes. This can be used as a guideline in practical applications for deciding which of these must be investigated in more detail and which can be neglected. Factors controlling nucleation, such as the interfacial tension or the contact angle, are experimentally under-determined in the respective geothermal in-situ conditions. In other words: the known range of the threshold supersaturation (Ω_{th}) is too uncertain in order to predict with the necessary precision whether heterogeneous nucleation will take place in a respective system (Fig. 2). Moreover, down-hole parameters, such as saturation state and specific surface area, are not measurable, but each constitutes a decisive impact on scaling mechanisms.

The parameter screening shows that parameters controlling nucleation have the overall largest impact on the model outcome. No detailed information is available with regard to minerals on the fracture wall, accessible to the fluid. While a contact angle of a barite nucleus on quartz, for example, is expected to be quite high due to their dissimilarity, a much smaller value can be assumed for similar crystal structures, such as celestite. However, detailed data on this is not available in the literature, and furthermore it would vary within a certain range, depending on the reservoir rock. Hence, the whole bandwidth of possible contact angles between a nucleus and substrate was evaluated. Interfacial tension γ also has a broad range, reported in the literature (Nielsen and Söhnel, 1971; Fernandez-Diaz et al., 1990; He et al., 1995; Prieto, 2014), and other studies have used it as a fitting parameter for models (e.g., Prieto, 2014; Poonoosamy et al., 2016). Furthermore, it

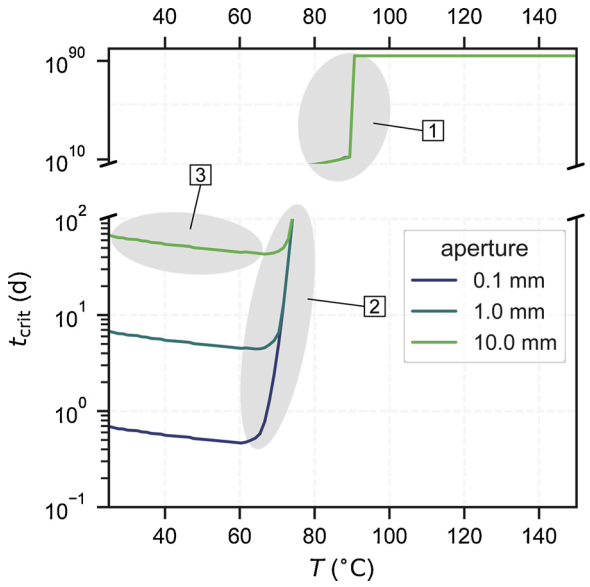

Fig. 9. Scenario for the Groß-Schönebeck site showing the time for permeability of a fracture to decrease by one order of magnitude (t_{crit}) at various apertures. (1): Supersaturation threshold is reached and nucleation begins (note $t_{crit} = 10^{94}$ d represents infinity.). (2): Whole fracture surface is covered with nucleations. (3): Kinetic rate constant decreases more than supersaturation increases. The input chemical state was taken from Table 2 (equilibrated at 150 °C). The model input file can be seen in Table B.5. (For interpretation of the references to color in this figure legend, the reader is referred to the web version of this article.)

becomes obvious from laboratory experiments (Fernandez-Diaz et al., 1990; He et al., 1995) that γ is a system dependent parameter. Although He et al. (1995) proposed a strong dependency on ionic strength and temperature, there still is no comprehensive study available on how to reliably predict γ at varying conditions.

Using the parameter ranges considered, the parameter screening shows that slightly more than 80% of the model-runs terminated because the threshold supersaturation was too high for nucleation to take place. From many experiments and observations it is known, however, that nucleation does take place at respective conditions in geothermal systems (e.g., Kühn et al., 1997; Regenspurg et al., 2015; Zhen-Wu et al., 2016). Currently, it is not possible to predict the threshold supersaturation for nucleation (Ω_{th}) with high enough certainty, so as to definitively foresee if it is overstepped in a system. Though, knowing Ω_{th} to a certain degree and its dependencies in a given system is crucial for a long-term operation because once nucleation has taken place, further permeability impairing crystal growth becomes more likely. It is further pointed out that, though heterogeneous nucleation is expected to be the dominant nucleation process, nucleation in the free solution is possible to some degree and is encouraged at increased flow velocities (Poonoosamy et al., 2020b). If these floating nuclei grow to sizeable colloids, clogging and decrease in rock permeability may take place. Thus, investigating these particular parameters in more detail could help to identify which of these can be manipulated in order to mitigate or even control nucleation. We refer to pertinent experimental studies (e.g., Zhen-Wu et al., 2016; Poonoosamy et al., 2016, 2020a), which are invaluable in narrowing down these uncertainties in geothermal conditions.

To further investigate the role of crystal growth, standard values for γ and θ with regard to barite nucleation in NaCl-solutions were used to fix these, as proposed by He et al. (1994). The resulting Ω_{th} is approximately 10, which coincides well with the results of experiments carried out by Zhen-Wu et al. (2016). There, evidence is reported for heterogeneous nucleation in a NaCl-solution at $\Omega = 32$, while none took place at $\Omega = 8$. Derived from the fluid composition at the Groß-Schönebeck site (Regenspurg et al., 2016), the expected barite supersaturation due to reduced temperatures is on the order of 30 (Fig. 3). Although some barite may precipitate along the surface system pathway, it is assumed that fluids will still be supersaturated when they are re-injected into the reservoir. In all three scenarios considered (Ω at 15, 20, and 30), Ω_{th} is overstepped and crystal growth determines the outcome of the models.

When crystal growth becomes the dominant mechanism ($\Omega > \Omega_{th}$), the scenarios outlined show that the parameters fracture aperture, salinity, and temperature are most influential for fracture sealing. The former coincides with the specific reactive surface area within a fracture, while the others influence the kinetic rate constant. This is an important point because the relative amount of fluid in contact with the fracture wall compared to the total amount of fluid in the fracture space is inversely proportional to the fracture aperture. It follows that the permeability of fractures with larger apertures is less affected by mineral scaling over time. More fluid volume can flow through before having the same permeability impairing effect, therefore larger apertures could be a reasonable approach for keeping injection rates stable for a longer period. Therefore, in terms of fracture sealing, a few large fractures are more favourable than producing a finely dendritic fracture network with an equivalent rock permeability.

Temperature and salinity have a strong impact on the precipitation mechanism (Risthaus et al., 2001; Zhen-Wu et al., 2016). Zhen-Wu et al. (2016) confirmed a previously postulated strong dependency of the rate constant on ionic strength (Risthaus et al., 2001) and temperature (Dove and Czank, 1995), as well as a negligible influence of pH in the range 5 to 7 (Ruiz-Agudo et al., 2015). The role of temperature in this sense is ambivalent. On the one hand, if fluids are cooled down, the respective supersaturation with regard to barite is increased, which is the main driving force for crystal growth and nucleation. On the other hand, the kinetic rate for crystal growth is reduced at lower temperatures. The impact of these two effects must be weighed up in detail for a specific system, so as to decide which is the ideal temperature. Of course, the necessary heat conversion must be taken into account. For the Groß-Schönebeck site, it was shown that cooling fluids down to 70 °C indeed can be seen as a worst case scenario with respect to barite scaling (Fig. 9). At these temperatures, the resulting supersaturation and nucleation rate will be high enough to cover the whole fracture surface, leading to a highly reactive surface area for crystal growth. Only at even lower temperatures will the rate constant decrease further to counter this effect to some extent. It should be noted that the threshold supersaturation was assumed to be 10 and that supersaturation is reached instantaneously at the fracture inlet.

Results show further that sealing rates are on the order of days or months (Table 4, Fig. 9). On average, these closing rates are by far smaller than the target life time of a geothermally utilised system (tens of years). Griffiths et al. (2016) came to a similar conclusion, who presented a model with regard to the geothermal site Soultz-sous-Forêts. They modelled radial growth of a seed barite crystal within a fracture in order to approximate sealing rates. For a fracture with an aperture of 20 mm, they derived a sealing time of about one month. Indeed, these rates are consistent with observations at various geothermal sites, where significant barite scale build-ups have been reported in the well bore and the surface system within months of production (Nitschke et al., 2014; Regenspurg et al., 2015; Griffiths et al., 2016). Regenspurg et al. (2015) report that approximately two tons of solids precipitated in the production well during the production of 20 000 m^3 fluids at the Groß-Schönebeck site; most of the residues in filters in the surface installation were composed of barite. They further report that this may have contributed to reduced flow rates over time.

5. Conclusions

This study assesses the impact of barite scaling on fracture permeability in the near field of the injection wells of geothermal systems by means of numerical simulations. It aims at illustrating the effects of

respective parameter ranges on scaling in fractures on the laboratory scale and aids in designing complementary laboratory experiments. The geothermal test-site Groß-Schönebeck is used as a basis, but the general physico-chemical conditions are applicable also to other sites, whose fluids exhibit increased Ba-supersaturation. For describing the precipitation mechanisms, a one-dimensional transport model is coupled with a two-step precipitation model that accounts for heterogeneous nucleation on fracture walls using classical nucleation theory as well as subsequent crystal growth kinetics using PHREEQC. A screening and sensitivity analysis with respect to fracture sealing times outlines, which of the hereby introduced parameters are most influential.

Nucleation and crystal growth both depend on supersaturation. Crystal growth is expected to only play a role, if nuclei have formed on the fracture wall. This happens if the respective threshold supersaturation is overstepped, which is determined by the interfacial tension and the contact angle. In the given range, these are the most influential parameters on the overall model outcome. In order to be able to predict the threshold supersaturation with sufficient certainty, these factors need to be determined in more detail in the laboratory and at in-situ conditions of geothermal applications.

Screening the parameter ranges shows that the threshold supersaturation is exceeded for a relevant chemical fluid composition, if temperature and pressure are reduced along the pathway of a geothermal power plant. In this case, crystal growth becomes the overall determining process, which is mainly controlled by the specific reactive surface area and the reaction mechanism. The surface area available in a fracture in proportion to the fluid is primarily defined by its aperture, while the rate constant depends on the fluid's temperature and salinity. The median times for fractures sealing are on the order of days or months. On average, these rates are considerably smaller than the economically required target life time of a geothermally utilised system, which is on the order of tens of years.

The results presented give time estimates for the impairing effect of barite scaling on fracture permeability and point out that they do pose a serious threat for the injectivity of geothermal wells, if the supersaturation threshold is exceeded. The lowering of temperature along the system pathway increases supersaturation and requires site specific assessment, as it also determines the amount of heat that can be harnessed. This is countered to some degree because lower temperatures also result in slower kinetic rates, hence these effects must be weighed up. The model outlined constitutes a tool for predicting and quantifying the temperature range, which is advisable for the fluid injection temperature. It is further advised rather to produce few fractures with large apertures than many with small apertures during hydraulic stimulation, so as to minimise sealing times.

CRediT authorship contribution statement

Morgan Tranter: Conceptualization, Methodology, Software, Validation, Formal Analysis, Investigation, Writing – Original Draft, Visualization.

Marco De Lucia: Methodology, Software, Writing – Review & Editing, Supervision.

Michael Kühn: Conceptualization, Writing – Review & Editing, Supervision, Project administration, Funding Acquisition.

Declaration of Competing Interest

The authors report no declarations of interest.

Acknowledgements

This research has been supported by the Federal Ministry for Economics and Energy of Germany BMWi (grant no. 0324244C, project ReSalt) and the Helmholtz Association of German Research Centres (grant no. ZT-I-0010, project Reduced Complexity Models).

Appendix A. Example PHREEQC input file

```
TITLE PhreeqSim
RATES
Barite # phreeqsim
-start
# (mol), temporary variable
10 moles = 0
# (mol m-2 s-1), dissolution rate constant
20 k_d = 10^PARM(1)
# (mol m-2 s-1), growth rate constant
30 k_p = 10^PARM(2)
40 sa = PARM(3) # (m2)
# (-), reaction order dissolution
50 n_d = 0.2
# (-), reaction order growth
60 n_p = 1.0
70 IF (SR("Barite") < 1.0)
AND (M <= 0.0) THEN GOTO 100
# Crystal dissolution
80 IF SR("Barite") < 1.0 THEN
moles = k_d * sa * (1 - SR("Barite")^_d)
# Crystal growth
90 IF SR("Barite") > 1.0 THEN
moles = k_p * sa * (1 - SR("Barite")^_p)
100 SAVE moles * TIME
-end
SELECTED_OUTPUT
-high_precision True
-reset false
USER_PUNCH
-headings step_no # base
-headings pH pe # sol
-headings Ba S Na Cl # element
-headings Ba+2 SO4-2 # species
-headings sr_Barite # sr_solid
-headings Barite # kin_solid
-start
10 PUNCH STEP_NO
20 PUNCH -LA('H+'), -LA('e-')
30 PUNCH TOT('Ba'), TOT('S'), TOT('Na'), TOT('Cl')
40 PUNCH MOL('Ba+2'), MOL('SO4-2')
50 PUNCH SR('Barite')
60 PUNCH KIN('Barite')
-end
END
#
==========================================-
======
SOLUTION 0
units mol/kgw
water 958.29329
temperature 60
pressure 98.692327
pH 6.0071915
pe 4
Ba 0.00089862195
S(6) 0.00089862195
Na 1.5
Cl 1.5
KINETICS 0
-steps 1 in 1 steps seconds
Barite
-m0 13.125398
-parms -5.96 -6.46 100000 # log_kd, log_kp, sa
END
```

Appendix B. Model input parameters

Table B.5

Table B.5
Transport model input parameters for the various sensitivity analysis and scenarios. OAT refers to the one-at-a-time parameter screening after Morris (Section 3.2). A, B, and C refer to the sensitivity analysis scenarios after Sobol (Section 3.3). GSB refers to the scenario for Groß-Schönebeck site (Section 3.4). Parameters: nodes (−), maximum time steps nt_{max} (−), length x (m), fracture aperture $\log d$ ($\log$ m), temperature T (°C), pressure $\log P$ ($\log$ Pa), flow velocity $\log u_x$ ($\log$ m s^{-1}), pH (−), elemental concentrations (mol kgw^{-1}), saturation state at inlet Ω_{in} (−), temperature at inlet T_{in} (°C), diffusion coefficient D_m (m^2 s^{-1}), interfacial energy γ (J m^{-2}), contact angle θ (°), molar volume V_m (cm^3 mol^{-1}). A single value means it was fixed. Two values mean it was varied uniformly in this range. If bc_T is not defined, it is the same as the domain temperature T.

Parameter	OAT (Morris)	A (Sobol)	B (Sobol)	C (Sobol)	GSB
nodes	6	6	6	6	6
nt_{max}	200	200	200	200	200
x	0.15	0.15	0.15	0.15	0.15
$\log d$	(-4, -2)	(-4, -2)	(-4, -2)	(-4, -2)	(-4, -2)
T	(50, 70)	(50, 70)	(50, 70)	(50, 70)	(25, 150)
$\log P$	(7.0, 7.7)	(7.0, 7.7)	(7.0, 7.7)	(7.0, 7.7)	7.7
$\log u_x$	(-3, 0)	(-3, 0)	(-3, 0)	(-3, 0)	−1
pH	(5, 7)	(5, 7)	(5, 7)	(5, 7)	5.7
Na^+	(0.1, 1.5)	(0.1, 1.5)	(0.1, 1.5)	(0.1, 1.5)	1.67
K^+	–	–	–	–	7.4×10^{-2}
Ca^{2+}	–	–	–	–	1.35
Mg^{2+}	–	–	–	–	1.8×10^{-2}
Ba^{2+}	–	–	–	–	2.469×10^{-3}
Sr^{2+}	–	–	–	–	2.2×10^{-2}
Cl^-	(0.1, 1.5)	(0.1, 1.5)	(0.1, 1.5)	(0.1, 1.5)	4.521
SO_4^{2-}	–	–	–	–	3.719×10^{-3}
HCO_3^-	–	–	–	–	3.1×10^{-4}
Ω_{in}	(1.1, 31.6)	15	20	30	1
T_{in}	–	–	–	–	150
D_m	1.0×10^{-9}	1.0×10^{-9}	1.0×10^{-9}	1.0×10^{-9}	1.0×10^{-9}
γ	(0.07, 0.134)	0.08	0.08	0.08	0.08
θ	(1, 179)	85	85	85	85
V_m	(50.26, 55.55)	(50.26, 55.55)	(50.26, 55.55)	(50.26, 55.55)	52.9

Appendix C. Supplementary data

Supplementary data associated with this article can be found, in the online version, at https://doi.org/10.1016/j.geothermics.2020.102027.

References

Appelo, C.A.J., 2015. Principles, caveats and improvements in databases for calculating hydrogeochemical reactions in saline waters from 0 to 200 °C and 1 to 1000 atm. Appl. Geochem. 55, 62–71. https://doi.org/10.1016/j.apgeochem.2014.11.007.

Appelo, C.A.J., Parkhurst, D.L., Post, V.E.A., 2014. Equations for calculating hydrogeochemical reactions of minerals and gases such as CO2 at high pressures and temperaturesGeochim. Cosmochim. Acta 125, 49–67. https://doi.org/10.1016/j.gca.2013.10.003.

Blöcher, G., Kluge, C., Milsch, H., Cacace, M., Jacquey, A.B., Schmittbuhl, J., 2019. Permeability of matrix-fracture systems under mechanical loading – constraints from laboratory experiments and 3-D numerical modelling. Adv. Geosci. 49, 95–104. https://doi.org/10.5194/adgeo-49-95-2019.

Blöcher, G., Reinsch, T., Henninges, J., Milsch, H., Regenspurg, S., Kummerow, J., Francke, H., Kranz, S., Saadat, A., Zimmermann, G., Huenges, E., 2016. Hydraulic history and current state of the deep geothermal reservoir Groß Schönebeck. Geothermics 63, 27–43. https://doi.org/10.1016/j.geothermics.2015.07.008.

Bozau, E., Häußler, S., Van Berk, W., 2015. Hydrogeochemical modelling of corrosion effects and barite scaling in deep geothermal wells of the North German Basin using PHREEQC and PHAST. Geothermics 53, 540–547. https://doi.org/10.1016/j.geothermics.2014.10.002.

Charlton, S.R., Parkhurst, D.L., 2011. Modules based on the geochemical model PHREEQC for use in scripting and programming languages. Comput. Geosci. 37, 1653–1663. https://doi.org/10.1016/j.cageo.2011.02.005.

Christy, A.G., Putnis, A., 1993. The kinetics of barite dissolution and precipitation in water and sodium chloride brines at 44-85 °C. Geochim. Cosmochim. Acta 57, 2161–2168. https://doi.org/10.1016/0016-7037(93)90557-D.

Dove, P.M., Czank, C.A., 1995. Crystal chemical controls on the dissolution kinetics of the isostructural sulfates: celestite, anglesite, and barite. Geochim. Cosmochim. Acta 59, 1907–1915. https://doi.org/10.1016/0016-7037(95)00116-6.

Fernandez-Diaz, L., Putnis, A., Cumberbatch, J., 1990. Barite nucleation kinetics and the effect of additives. Eur. J. Mineral. 2, 495–501.

Griffiths, L., Heap, M.J., Wang, F., Daval, D., Gilg, H.A., Baud, P., Schmittbuhl, J., Genter, A., 2016. Geothermal implications for fracture-filling hydrothermal precipitation. Geothermics 64, 235–245. https://doi.org/10.1016/j.geothermics.2016.06.006.

He, S., Oddo, J.E., Tomson, M.B., 1994. The inhibition of gypsum and barite nucleation in NaCl brines at temperatures from 25 to 90 °C. Appl. Geochemistry 9, 561–567. https://doi.org/10.1016/0883-2927(94)90018-3.

He, S., Oddo, J.E., Tomson, M.B., 1995. The nucleation kinetics of Barium Sulfate in NaCl solution up to 6 m and 90 °C. J. Colloid Interface Sci. 319–326.

Heberling, F., Schild, D., Degering, D., Schäfer, T., 2017. How well suited are current thermodynamic models to predict or interpret the composition of (Ba,Sr)SO_4 solid-solutions in geothermal scalings? Geotherm. Energy 5. https://doi.org/10.1186/s40517-017-0068-x.

Hörbrand, T., Baumann, T., Moog, H.C., 2018. Validation of hydrogeochemical databases for problems in deep geothermal energy. Geotherm. Energy 6, 20. https://doi.org/10.1186/s40517-018-0106-3.

Kashchiev, D., 2000. Nucleation: Basic Theory With Applications. Butterworth Heinemann, Oxford, Boston.

Kühn, M., Frosch, G., Kölling, M., Kellner, T., 1997. Experimentelle Untersuchungen zur Barytübersättigung einer Thermalsole. Grundwasser 2, 111–117. https://doi.org/10.1007/s767-1997-8532-2.

Lasaga, A.C., 1998. Kinetic Theory in the Earth Sciences. Princeton University Press.

Liu, X.Y., 1999. A new kinetic model for three-dimensional heterogeneous nucleation. J. Chem. Phys. 111, 1628–1635. https://doi.org/10.1063/1.479391.

Morris, M.D., 1991. Factorial sampling plans for preliminary computational experiments. Technometrics 33, 161–174. https://doi.org/10.1080/00401706.1991.10484804.

Neuzil, C.E., Tracy, J.V., 1981. Flow through fractures. Water Resour. Res. 17, 191–199. https://doi.org/10.1029/WR017i001p00191.

Nielsen, A.E., 1964. Kinetics of Precipitation. Pergamon, Oxford, Oxford.

Nielsen, A.E., Söhnel, O., 1971. Interfacial tensions electrolyte crystal-aqueous solution, from nucleation data. J. Cryst. Growth 11, 233–242. https://doi.org/10.1016/0022-0248(71)90090-X.

Nitschke, F., Scheiber, J., Kramar, U., Neumann, T., 2014. Formation of alternating layered Ba-Sr-sulfate and Pb-sulfide scaling in the geothermal plant of Soultz-sous-For ê ts. Neues Jahrb. für Mineral. – Abhandlungen J. Mineral. Geochem. 191, 145–156. https://doi.org/10.1127/0077-7757/2014/0253.

Palandri, J.L., Kharaka, Y.K., 2004. A Compilation of Rate Parameters of Water-Mineral Interaction Kinetics for Application to Geochemical Modeling. https://doi.org/10.1098/rspb.2004.2754. USGS Open File Rep. 2004-1068, 71. arXiv:ADA440035.

Parkhurst, D.L., Appelo, C.A.J., 2013. Description of Input and Examples for PHREEQC Version 3: A Computer Program for Speciation, Batch-Reaction, One-Dimensional Transport, and Inverse Geochemical Calculations. https://doi.org/10.3133/tm6A43. Technical Report. Reston, VA.

Pitzer, K.S., 1973. Thermodynamics of electrolytes. I. Theoretical basis and general equations. J. Phys. Chem. 77, 268–277. https://doi.org/10.1021/j100621a026.
Poonoosamy, J., Curti, E., Kosakowski, G., Grolimund, D., Van Loon, L., Mäder, U., 2016. Barite precipitation following celestite dissolution in a porous medium: a SEM/BSE and μ-XRD/XRF study. Geochim. Cosmochim. Acta 182, 131–144. https://doi.org/10.1016/j.gca.2016.03.011.
Poonoosamy, J., Klinkenberg, M., Deissmann, G., Brandt, F., Bosbach, D., Mäder, U., Kosakowski, G., 2020a. Effects of solution supersaturation on barite precipitation in porous media and consequences on permeability: experiments and modelling. Geochim. et Cosmochim. Acta 270, 43–60. https://doi.org/10.1016/j.gca.2019.11.018.
Poonoosamy, J., Soulaine, C., Burmeister, A., Deissmann, G., Bosbach, D., Roman, S., 2020b. Microfluidic flow-through reactor and 3D Raman imaging for in situ assessment of mineral reactivity in porous and fractured porous media. Lab Chip 20, 2562–2571. https://doi.org/10.1039/D0LC00360C.
Prieto, M., 2014. Nucleation and supersaturation in porous media (revisited). Mineral. Mag. 78, 1437–1447. https://doi.org/10.1180/minmag.2014.078.6.11.
Regenspurg, S., Feldbusch, E., Byrne, J., Deon, F., Driba, D.L., Henninges, J., Kappler, A., Naumann, R., Reinsch, T., Schubert, C., 2015. Mineral precipitation during production of geothermal fluid from a Permian Rotliegend reservoir. Geothermics 54, 122–135. https://doi.org/10.1016/j.geothermics.2015.01.003.
Regenspurg, S., Feldbusch, E., Norden, B., Tichomirowa, M., 2016. Fluid-rock interactions in a geothermal Rotliegend/Permo-Carboniferous reservoir (North German Basin). Appl. Geochem. 69, 12–27. https://doi.org/10.1016/j.apgeochem.2016.03.010.
Regenspurg, S., Wiersberg, T., Brandt, W., Huenges, E., Saadat, A., Schmidt, K., Zimmermann, G., 2010. Geochemical properties of saline geothermal fluids from the in-situ geothermal laboratory Groß Schönebeck (Germany). Chemie der Erde 70, 3–12. https://doi.org/10.1016/j.chemer.2010.05.002.
Risthaus, P., Bosbach, D., Becker, U., Putnis, A., 2001. Barite scale formation and dissolution at high ionic strength studied with atomic force microscopy. Colloids Surfaces A Physicochem. Eng. Asp. 191, 201–214. https://doi.org/10.1016/S0927-7757(00)00843-8.
Ruiz-Agudo, C., Putnis, C.V., Ruiz-Agudo, E.ó.n., Putnis, A., 2015. The influence of pH on barite nucleation and growth. Chem. Geol. 391, 7–18. https://doi.org/10.1016/j.chemgeo.2014.10.023.
Saltelli, A., 2002. Making best use of model evaluations to compute sensitivity indices. Comput. Phys. Commun. 145, 280–297. https://doi.org/10.1016/S0010-4655(02)00280-1.
Scheiber, J., Seibt, A., Birner, J., Genter, A., Moeckes, W., 2013. Application of a scaling inhibitor system at the geothermal power plant in Soultz-sous-Forê ts: laboratory and on-site studies. Eur. Geotherm. Congr. 2013, 1–10.
Seibt, P., Kabus, F., Wolfgramm, M., Bartels, J., Seibt, A., 2010. Monitoring of hydrogeothermal plants in Germany – an overview. Proc. World Geotherm. Congr. 7.
Sobol, I., 2001. Global sensitivity indices for nonlinear mathematical models and their Monte Carlo estimates. Math. Comput. Simul. 55, 271–280. https://doi.org/10.1016/S0378-4754(00)00270-6.
Steefel, C.I., 2008. Geochemical Kinetics and Transport. Springer New York, New York, NY, pp. 545–589. https://doi.org/10.1007/978-0-387-73563-4_11.
Stober, I., Wolfgramm, M., Birner, J., 2013. Hydrochemie der Tiefenwässer in Deutschland. Zeitschrift für Geol. Wissenschaften 42, 339–380.
Tesmer, M., Möller, P., Wieland, S., Jahnke, C., Voigt, H., Pekdeger, A., 2007. Deep reaching fluid flow in the North East German basin: origin and processes of groundwater salinisation. Hydrogeol. J. 15, 1291–1306. https://doi.org/10.1007/s10040-007-0176-y.
Wolfgramm, M., Rauppach, K., Seibt, P., 2008. Reservoir-geological characterization of Mesozoic sandstones in the North German Basin by petrophysical and petrographical data. Zeitschrift für Geol. Wissenschaften 249–265.
Wolfgramm, M., Rauppach, K., Thorwart, K., 2011a. Mineralneubildung und Partikeltransport im Thermalwasserkreislauf geothermischer Anlagen Deutschlands. Zeitschrift für Geol. Wissenschaften 39, 213–239.
Wolfgramm, M., Thorwart, K., Kerstin, R., Brandes, J., 2011b. Zusammensetzung, Herkunft und Genese geothermaler Tiefengrundwässer im Norddeutschen Becken (NDB) und deren Relevanz für die geothermische Nutzung. Zeitschrift für Geol. Wissenschaften 173–193.
Zhen-Wu, B.Y., Dideriksen, K., Olsson, J., Raahauge, P.J., Stipp, S.L., Oelkers, E.H., 2016. Experimental determination of barite dissolution and precipitation rates as a function of temperature and aqueous fluid composition. Geochim. Cosmochim. Acta 194, 193–210. https://doi.org/10.1016/j.gca.2016.08.041.
Zimmermann, G., Moeck, I., Blöcher, G., 2010. Cyclic waterfrac stimulation to develop an enhanced geothermal system (EGS)-conceptual design and experimental results. Geothermics 39, 59–69. https://doi.org/10.1016/j.geothermics.2009.10.003.